Phase-shifting point-diffraction interferometry at 193 nm

Sang Hun Lee, Patrick Naulleau, Kenneth A. Goldberg, Fan Piao, William Oldham, and Jeffrey Bokar

Phase-shifting point-diffraction interferometry at the 193-nm wavelength suitable for highly accurate measurement of wave-front aberration is introduced. The interferometer preserves the advantages of the previously described extreme-ultraviolet phase-shifting point-diffraction interferometer but offers higher relative efficiency. Wave-front measurement of an imaging system, operating at the 193-nm wavelength, is reported. Direct measurement of the refractive-index change in a deep-ultraviolet radiation-damaged fused-silica sample is also presented as an application. © 2000 Optical Society of America

OCIS codes: 120.3180, 050.5080, 120.3940, 120.5050, 030.1640, 350.2770, 110.3960.

1. Introduction

The desire for high-quality optics places stringent requirements on the accuracy of interferometers used for optical metrology. Wave-front measurement at the operational wavelength of an optical system plays an important role in system performance characterization. To provide high-accuracy wave-front measurements at short wavelengths, the phase-shifting point-diffraction interferometer (PS/PDI) was recently developed.[1–5] The PS/PDI design preserves the advantages of the conventional point-diffraction interferometer[6,7] yet allows for phase-shifting capability and higher throughput.[1] Because the PS/PDI is a common-path interferometer, it is stable, resistant to vibration, and appropriate for light sources with moderate longitudinal coherence.

The PS/PDI was initially developed for wave-front characterization of extreme-ultraviolet (EUV) lithographic optics operating at wavelengths near 13.4 nm.[2,3] Here we implement an alternate configuration of the PS/PDI optimized for operation at the wavelength of 193 nm.

The configuration of the EUV PS/PDI is depicted in Fig. 1(a). The EUV PS/PDI consists of an object pinhole, a transmission grating, a pair of pinholes in the image-plane pinhole mask, and a CCD detector. Spatially coherent spherical-wave illumination is provided by diffraction from the object pinhole. The transmission grating serves as a small-angle beam splitter providing the test and the reference beams required for the interferometry. The optic under test focuses the various grating orders to the image plane. One pinhole in the image plane generates the reference beam by spatial filtering of one of the grating diffracted orders; the test beam, however, propagates, largely unaffected, through a relatively large second pinhole, or window, as shown in Fig. 1(a). The rest of the grating orders are blocked by the opaque membrane containing the pinholes. The test and the reference beams propagate to the mixing (CCD) plane where they overlap to create an interference pattern. The interferogram is thus a comparison of the test beam with the ideally spherical reference wave. Phase shifting can be achieved by translation of the grating, which produces a controllable relative phase shift between the orders of the grating.

Errors in the grating line placement can be filtered if the first order of the grating is used as the reference beam. However, because the first-order beam is weaker than the zeroth order when an amplitude grating is used as is in this case, and because pinhole filtering can attenuate the beam significantly, use of

S. H. Lee (shlee@lbl.gov), W. Oldham, and F. Bokor are with the Department of Electrical Engineering and Computer Sciences, University of California, Berkeley, Berkeley, California 94720. S. H. Lee, P. Naulleau, K. A. Goldberg, and J. Bokor are with the Center for X-Ray Optics, Lawrence Berkeley National Laboratory, Berkeley, California 94720. F. Piao is with the Department of Materials Science and Mineral Engineering, University of California, Berkeley, Berkeley, California 94720.

Received 21 April 2000; revised manuscript received 6 July 2000.
0003-6935/00/315768-05$15.00/0

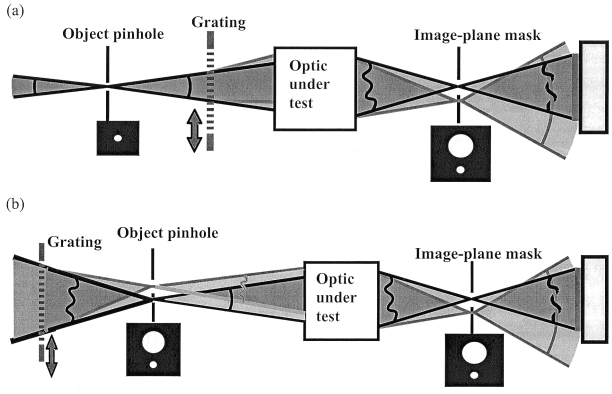

Fig. 1. (a) Schematic diagram of conventional PS/PDI configuration used at EUV wavelengths to test lithographic optics. The grating is placed after the object pinhole. (b) Schematic diagram of the upstream-grating PS/PDI configuration used at the 193-nm wavelength. Placement of the grating before the object-plane pinhole improves the throughput of the interferometer.

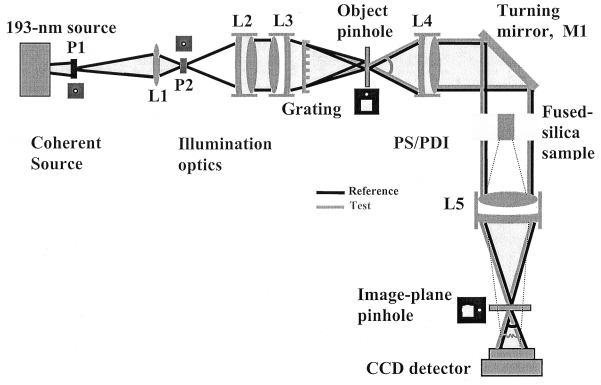

Fig. 2. Experimental configuration of the 193-nm PS/PDI. The turning mirror is required because of space constraint. L, lens; M, mirror; P, pinhole.

the first-order beam as the reference can lead to low fringe contrast.

To improve the fringe contrast while maintaining suppression of grating-line-placement error, an alternate configuration of the PS/PDI[1,8] was proposed with the grating placed before the object plane [Fig. 1(b)]. Since the reference and the test beams are each spatially filtered once, fringe contrast exceeding 90% is readily achieved. Also, the fact that the spatial filtering is performed after passage through the grating allows for suppression of grating-line-placement errors. This design, however, is limited to use when the beam delivery system illuminating the object plane can provide a small image spot relative to the grating-induced beam separation at the object plane. We note that this is not the case for the EUV PS/PDI when an undulator beamline is used as the beam delivery system,[2,3] but it can be the case at the 193-nm wavelength, where conventional lasers and lenses are used.

In the upstream-grating PS/PDI configuration [Fig. 1(b)] an illumination system is used to produce a focused spot in the object plane of the optic under test. A coarse grating placed before the object plane is inserted into the illumination system to act as a beam splitter, producing multiple laterally displaced foci in the object plane. A mask containing a spatial-filtering pinhole and a large window is placed in the object plane to select two of the orders diffracted by the grating. The weaker first-order beam passes unattenuated through the window and will eventually serve as the reference beam. The zeroth-order beam is spatially filtered by the pinhole providing nearly perfect spherical-wave illumination used as the test beam.

The two beams propagate through the optic under test, acquiring aberrations imparted by the optic, and are focused in the image plane. A second mask located in the image plane contains a window and small pinhole. Here the test beam passes through the relatively large window, and the reference beam is filtered by the small pinhole.

In summary, for the upstream-grating PS/PDI each beam is filtered only once: The test beam is filtered in the object plane, and the reference beam is filtered in the image plane. In this way the reference beam reaches the image plane with much greater intensity than in the conventional PS/PDI design, and any potential aberrations introduced by the grating can be filtered.

Another significant advantage of the upstream-grating configuration is that it provides beam equalization, allowing high-contrast interferograms to be recorded, and thereby improving the signal-to-noise ratio of the measurement. Beam power balancing is achieved by proper selection of the relative sizes of the spatial-filtering pinholes in the object and the image planes. This cannot be easily achieved in the other configuration, in which the reference and the test beams both effectively experience the same losses from the object-plane pinhole, unless the zeroth order is used as the reference beam and suppression of grating-line-placement error is sacrificed.

Here we describe the implementation of an upstream-grating PS/PDI operating at the 193-nm wavelength. The interferometer is used to characterize the wave front of a 193-nm imaging system. Furthermore, the system is designed to study deep-ultraviolet (DUV) radiation-induced refractive-index changes in flat fused-silica samples.

2. Phase-Shifting Point-Diffraction Interferometry Setup at 193 nm

The upstream-grating PS/PDI described above was implemented as shown in Fig. 2. The interferometer is designed to test an optical imaging system with numerical aperture (NA) as large as 0.11. The setup is divided into three parts: a coherent source, illumination optics, and the PS/PDI.

The illumination is provided by a Lambda-Physik Model LPX-140I pulsed ArF excimer laser operating at 193 nm. This laser provides pulse widths of approximately 18 ns (FWHM) at 150 Hz and can be

operated at repetition rates as high as 400 Hz with a maximum power output of 60 W.

Because of the relatively low spatial coherence of the excimer laser, spatial filtering was required for providing sufficiently coherent illumination of the interferometer. To avoid laser damage of pinhole spatial filters (intense excimer laser pulses readily ablate pinholes), a dual-pinhole filtering scheme (Fig. 2) was used. A 50-μm-diameter pinhole (P1) is placed in the raw beam approximately 15 cm from the source to select approximately one spatial coherence diameter. This first filtering stage causes a pulse energy reduction of 2×10^{-5}. The illumination is further spatially filtered by the lens (L1) and 5-μm-diameter pinhole (P2) combination. A pair of doublet lenses (L2, L3) are used to reimage pinhole P1 to the PS/PDI object plane. A 400-μm-pitch chrome-on-glass diffraction grating is placed between L3 and the object plane to act as a beam splitter, providing a 120-μm beam separation in the object plane.

The object-plane mask consists of a 120-μm square window and a 2-μm pinhole. The window-to-pinhole center-to-center separation is 120 μm. The pinhole is centered on the focus of the zeroth diffracted order of the grating, thus removing aberrations imparted by the upstream optics and generating the spherical test beam. The window is positioned to selectively pass the first diffracted order of the grating, which will eventually serve as the reference beam.

The optical imaging system is a combination of L4, mirror M1, and L5 with unit magnification. Lenses L4 and L5 are commercial DUV, high-quality doublet lenses made of fused silica. Their focal lengths are both 20.5 cm at a 193-nm wavelength. Mirror M1 is a fused-silica-based mirror optically coated to have its peak reflectivity (95%) at a 193-nm wavelength at a 45° angle of incidence.

The image-plane mask design is identical to the object-plane mask except that the positions of the pinhole and the window are reversed. The test beam carrying the aberrations imparted by the optical system under test propagates nearly unaffected through the window. The reference beam is focused onto the pinhole where it is spatially filtered to provide a spherical reference wave with which the test beam is interferometrically compared.

3. Experimental Results

The interferometer measures the overall aberrations in the optical system under test, a combination of lenses L4 and L5 and mirror M1. A representative interferogram is shown in Fig. 3(a). The fringe contrast is approximately 90%. With a five-bucket phase-shifting method[9] the measured wave-front phase map over 0.035 NA, with piston, tilt, and defocus removed, is shown in Fig. 3(b). The 36-term Zernike polynomial decomposition of the resulting wave front is shown in Fig. 3(c). The dominant wave-front errors are 0.085 λ of coma and 0.078 λ of astigmatism. The peak-to-valley aberration and rms magnitude of the overall wave front is 0.30 λ (57.90 nm) and 0.050 λ (9.65 nm), respectively. The same imaging system was independently measured over 50 times, revealing a measurement repeatability of 0.004 λ (0.77 nm) rms.

4. Testing Deep-Ultraviolet Damaged Fused-Silica Samples

Recently the industrial standard critical dimension for integrated-circuit devices dropped from 0.25 to 0.18 μm. Further progress to critical dimensions of 0.18 and 0.13 μm are anticipated by reduction of wavelength used in the optical lithography step from 248 to 193 nm.[10] At the 193-nm wavelength the choice of optical materials for lenses is limited essentially to fused silica and CaF_2. For reasons of homogeneity, cost, and availability, the former is preferred. However, fused silica is subject to both irradiation-induced color-center formation and compaction at DUV wavelengths.[10–14] Compaction introduces phase aberrations in lithographic optical systems, owing both to the change in refractive index of the compacted area and the geometric path-length change through the optic.[10]

By use of the 193-nm PS/PDI, lens materials can be directly and quantitatively evaluated at their intended operational wavelength, where changes in the optical path length can be investigated. For example, the effects of DUV radiation damage on fused silica can be characterized interferometrically.

As a demonstration of this capability we tested a flat sample of fused silica (type B, supplied by SEMATECH)[15] both before and after DUV damage. The flat sample had dimensions of 4 cm × 2 cm × 1 cm and was polished on all six surfaces. Transmission through the sample was tested over a 15-mm-diameter region, where the beam propagates in the 1-cm direction.

The damaged fused-silica sample was placed between mirror M1 and the final lens of the system (L5) at which point the beams are collimated. One of the recorded interferograms from the phase-shifting series is shown in Fig. 4(a). The corresponding wave front is shown in Fig. 4(b). The wave front shown in Fig. 4(b) includes aberrations imparted by L4, M1, L5, and the damaged fused-silica sample. However, because we measured the undamaged fused-silica sample first, which includes the aberrations from L4, M1, L5, and the undamaged fused-silica sample, we can identify the net effect caused by radiation damage by differencing two measurements. A peak refractive-index change of 1.6 parts per million was measured for this particular sample. A detailed description of this study has been published elsewhere.[15]

5. Extendability to the 157-nm Wavelength

It is widely believed that optical lithography will eventually be extended to the 157-nm wavelength. The most promising lens material for 157-nm lithography is CaF_2; however, this material may also experience various types of DUV radiation-induced

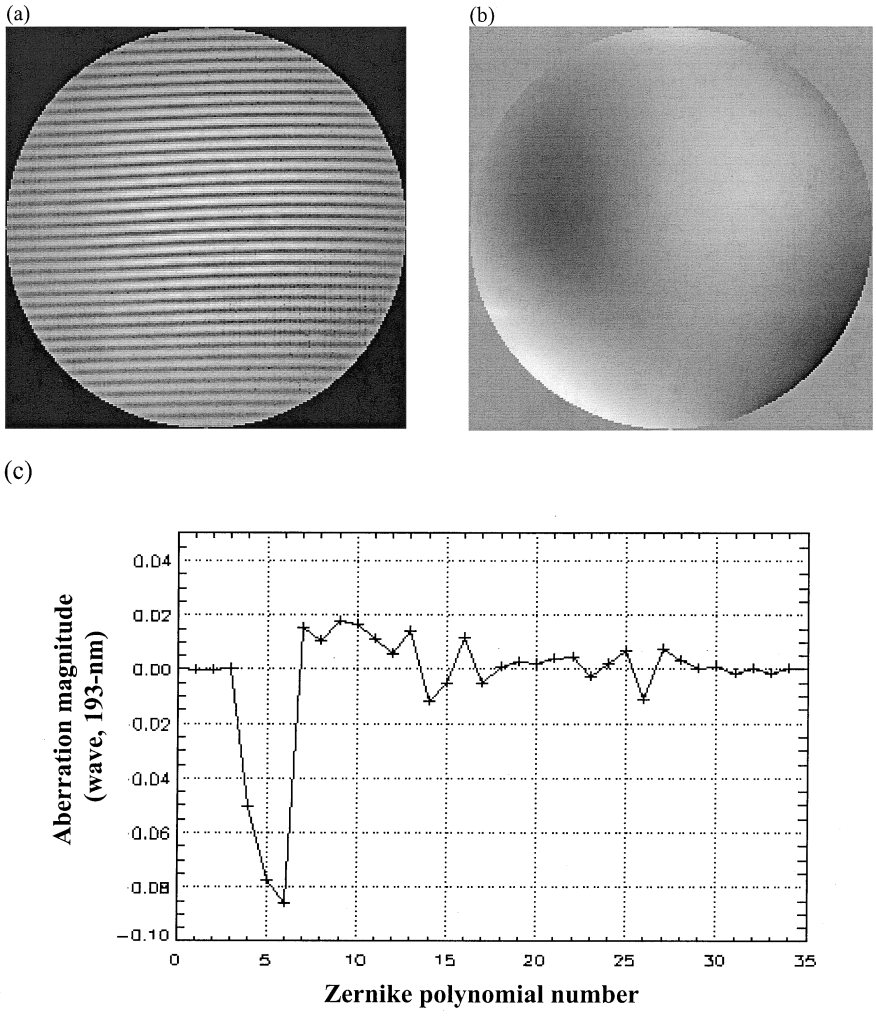

Fig. 3. (a) Representative interferogram obtained during testing of the optical imaging system comprised of lenses L4 and L5 and mirror M1. (b) Resultant wave front: The peak-to-valley wave-front error is 0.3 waves and the rms error is 0.05 waves at 193-nm wavelength over a 0.035 NA. (c) Thirty-six Zernike polynomial decomposition of the wave front; the most significant term is coma.

damage. The upstream-grating PS/PDI could easily be adapted for use at the 157-nm wavelength for direct measurement of radiation-induced CaF_2 damage. The pinhole sizes could be scaled down appropriately to meet the wavelength and NA requirements, and fused-silica-based optics used in the 193-nm PS/PDI must, of course, be replaced with CaF_2-based optics.

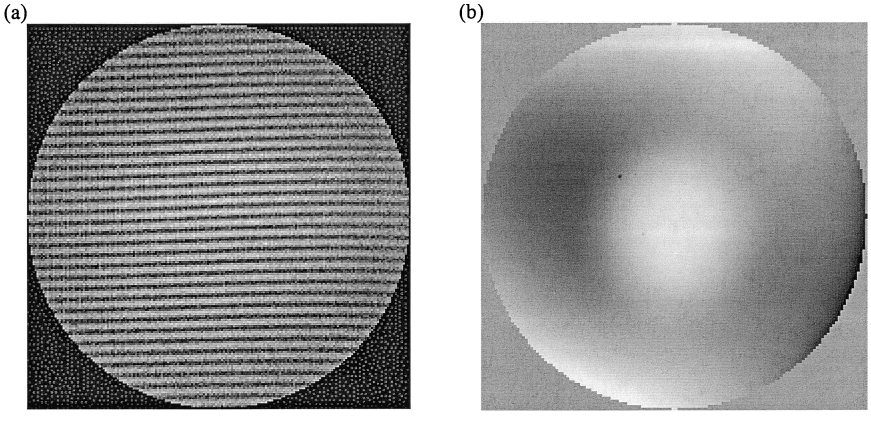

Fig. 4. (a) Representative interferogram obtained with the damaged fused-silica sample installed. (b) Resultant wave front indicating a damaged region at the center of the 15-mm-diameter test area.

6. Conclusion

A 193-nm phase-shifting point-diffraction interferometer (PS/PDI) has been demonstrated for the first time to our knowledge. High-contrast fringes with the upstream-grating PS/PDI design have been achieved. An imaging lens system and a DUV damaged fused-silica sample have been successfully tested with the interferometer. Measurement repeatability of 0.004λ rms has been achieved. Future research should include more detailed accuracy characterization and investigation of the extendability to higher-NA imaging systems.

The authors thank Edita Tejnil for innumerable contributions in designing the PS/PDI at 193 nm. This research was jointly sponsored under Semiconductor Research Corporation (SRC) contract 96-LC-460 and Defense Advanced Research Projects Agency (DARPA) grant MDA972-97-1-0010.

References

1. H. Medecki, E. Tejnil, K. A. Goldberg, and J. Bokor, "Phase-shifting point diffraction interferometer," Opt. Lett. **21,** 1526–1528 (1996).
2. E. Tejnil, K. A. Goldberg, S. H. Lee, H. Medecki, P. J. Batson, P. E. Denham, A. A. MacDowell, and J. Bokor, "At-wavelength interferometry for EUV lithography," J Vac. Sci. Technol. B **15,** 2455–2461 (1997).
3. K. Goldberg, P. Naulleau, and J. Bokor, "EUV interferometric measurements of diffraction-limited optics," J. Vac. Sci. Technol. B **17,** 2982–2986 (1999).
4. P. Naulleau, K. A. Goldberg, S. H. Lee, C. Chang, C. Bresloff, P. Batson, D. Attwood, and J. Bokor, "Characterization of the accuracy of EUV phase-shifting point diffraction interferometry," in *Emerging Lithographic Technologies II*, Y. Vladimirsky, ed., Proc. SPIE **3331,** 114–123 (1998).
5. P. P. Naulleau, K. A. Goldberg, S. H. Lee, C. Chang, D. Attwood, and J. Bokor, "Extreme-ultraviolet phase-shifting point-diffraction interferometer: a wave-front metrology tool with subangstrom reference-wave accuracy," Appl. Opt. **38,** 7252–7263 (1999).
6. W. Linnk, "A simple interferometer to test optical systems," Proc. Acad. Sci. USSR **1,** 210–212 (1933).
7. R. N. Smartt and W. H. Steel, "Theory and application of point diffraction interferometers," Japan. J. Appl. Phys. **14,** Suppl. 14-1, 351–356 (1975).
8. K. Goldberg, "EUV interferometry," Ph.D. dissertation (Department of Physics, University of California, Berkeley, Berkeley, Calif., 1997).
9. D. Malacara, ed., *Optical Shop Testing* (Wiley, New York, 1992).
10. W. G. Oldham and R. E. Schenker, "193-nm lithographic system lifetimes as limited by UV compaction," Solid State Technol. **40,** 95–102 (1997).
11. M. Rothschild, D. J. Ehrlich, and D. C. Shaver, "Effects of excimer laser irradiation on the transmission, index of refraction, and density of ultraviolet grade fused silica," Appl. Phys. Lett. **55,** 1276–1278 (1989).
12. D. C. Allan, C. Smith, N. F. Borrelli, and T. P. Seward III, "193-nm excimer-laser-induced densification of fused silica," Opt. Lett. **21,** 1960–1962 (1996).
13. R. Schenker and W. G. Oldham, "Ultraviolet-induced densification in fused silica," J. Appl. Phys. **82,** 1065–1071 (1997).
14. F. Piao, R. Schenker, and W. G. Oldham, "Temperature dependence of UV-induced compaction in fused silica," in *Optical Microlithography X*, G. E. Fuller, ed., Proc. SPIE **3051,** 907–912 (1997).
15. S. Lee, F. Piao, P. Naulleau, K. Goldberg, W. Oldham, and J. Bokor, "At-wavelength characterization of DUV-radiation-induced damage in fused silica," in *Metrology, Inspection, and Process Control for Microlithography XIV*, N. T. Sullivan, ed., Proc. SPIE **3998,** 724–731 (2000).